J Electr Eng Technol.2018; 13(3): 1156-1165
http://doi.org/10.5370/JEET.2018.13.3.1156

ISSN(Print) 1975-0102
ISSN(Online) 2093-7423

High-Performance Elevator Traction Using Direct Torque Controlled Induction Motor Drive

Osama Mohamed Arafa*, Mohamed Elsayed Abdallah and Ghada Ahmed Abdel Aziz†**

Abstract – This paper presents a detailed realization of direct torque controlled induction motor drive for elevator applications. The drive is controlled according to the well-known space vector modulated direct control scheme (SVM-DTC). As the elevator drives are usually equipped with speed sensors, flux estimation is carried out using a current model where two stator currents are measured and accurate instantaneous rotor speed measurement is used to overcome the need for measuring stator voltages. Speed profiling for a comfortable elevator ride and other supervisory control activities to provide smooth operation are also explained. The drive performance is examined and controllers' parameters are fine-tuned using MATLAB/SIMULINK. The blocks used for flux and torque estimation and control in the offline simulation are compiled for real-time using dSPACE Microlabox. The performance of the drive has been verified experimentally. The results show good performance under transient and steady state conditions.

Keywords: Direct Torque Control (DTC), DSP, Elevator drives, Induction motor drives, Stator voltage reconstruction, Voltage source inverter nonlinearity.

1. Introduction

Direct torque control (DTC) as a robust, rapid-responding control strategy is a good candidate for squirrel cage induction machine (SCIM) drives in elevator applications [1]. As the type of high-speed elevator systems alter, standardization of the electrical drive systems is indispensable. General requirements of the elevator drive system include the more convenient ride, accurate and effective speed control, energy saving, and reliability [2]. The DTC control strategy can ensure faster torque response while maintaining the stator flux linkage and torque decoupled compared with scalar control [3].

Although in principle, DTC follows the flux orientation philosophy, it has its unique features compared to vector control methods. It needs no coordinate transformation, less sensitivity to the IM parameters is easily realized, and hence DTC allows direct control of the motor torque by an appropriate selection of the inverter control sequences in the DTC scheme [4].

The original DTC scheme proposed earlier by Takahashi and Nougouchi in 1986 got the error signals by estimating the IM's developed torque and flux linkage based on some measurements and known motor parameters and compared them with the desired torque and flux linkage values. Flux and torque errors were used to drive hysteresis controllers whose outputs decide the desired stator voltage space vector by fetching predefined switching lookup tables [5]. Although conventional DTC with hysteresis controller strategy has the merits of simple structure, rapid response, and low reliance on IM parameters, it is characterized with two main disadvantages [6]. The first is that the switching frequency varies depending on the motor speed and the width of the hysteresis bands of torque and flux. The second is that it is rendered with considerable torque ripples [7]. Thus, it provides noticeably poor performance at low speeds. The latter issue is problematic for elevators where speed range extends from zero to rated speed in both forward and reverse directions and the speed should be varied in a soft and smooth manner.

Since its introduction, the original DTC scheme has undergone several developments to improve it and to overcome its weaknesses and disadvantages. Consequently, the DTC strategies available today can be classified into four main categories: 1) strategies considering variable hysteresis band controllers [8]; 2) strategies with space vector modulation (SVM-DTC) [9]; 3) strategies using predictive control schemes [10]; and 4) strategies built around artificial intelligent control approaches [10].

In the traditional switching-table based DTC schemes (ST-DTC), there are 60° sectors of both flux linkage and voltage vectors, which produce a high torque ripple. The torque ripple can be reduced by increasing number of levels of the torque comparator and increasing the degrees of freedom for selection of proper vectors. A new ST-DTC scheme based on the direct matrix converter (DMC) using a twelve-side polygonal space vector (SV) for variable speed control of an IM has been introduced in [11]. The DMC method utilizes twelve 30° sectors of both flux

† Corresponding Author: Dept. of Power Electronics & Energy Conversion, Electronics Research Institute, Egypt. (oarafa@eri.sci.eg)
* Dept. of Power Electronics & Energy Conversion, Electronics Research Institute , Egypt. ({eng.msa12, ghada_ahmed}@eri.sci.eg)
Received: August 22, 2017; Accepted: November 6, 2017

linkage and voltage vectors doubling the number of sectors traditionally available.

Artificial intelligence (AI) based systems have been used for improving the performance of the conventional ST-DTC scheme. Some of them are; duty ratio control using fuzzy inference system (FIS), direct selection of inverter state by fuzzy [12], neuro-fuzzy controllers (NFC) [7], and artificial neural network (ANN) control based-DTC [13].

Together with multi-level torque comparators, multi-level inverters (more than 2 levels), and multi-phase machines (more than three phase) have also been used to overcome the torque ripple problem of DTC schemes. In [14], a seven-level torque comparator has been used for minimizing the torque ripple in the DTC-controlled five-phase IM fed by a three-level five-phase. In [15], a three-level neutral point clamped (TL-NPC) inverter based-DTC of a five-phase induction motor (FPIM) has been presented. The main merits of the three-level inverter over two-levels one for DTC operation is the low torque ripple effect. Also, the TL-NPC inverter through SVM technique enjoys low *dv/dt* transitions with smooth voltage waveform.

The variable switching frequency issue is fixed by applying SVM concept. In [16], an improved DTC-SVM using over-modulation technique has been proposed. This technique produces a minimum torque ripple and improves the power factor. An improved SM-DTC scheme based on second order sliding-mode controllers and space vector modulation for IM drive has been introduced in [17]. The reference voltages direct and quadrature components have been generated based on decoupled super twisting controllers for stator flux linkage and electromagnetic torque control. This combined algorithm has been designed to overcome the drawbacks belonging to DTC control scheme. It is concluded that the constant switching frequency DTC-SVM scheme in [18] improves drive performance considerably in terms of reduced torque and flux pulsations, limits stator phase current, and provides reliable low-speed operation.

A new predictive direct torque controller (PDTC) for IMs has been proposed in [19]. The proposed PDTC used Kalman filter for reliable flux estimation and reducing the measurement noise. The main drawback of this technique is its dependence on the accurate IM parameters.

A new feedback linearization approach has been introduced in [20]. This approach offers a decoupled linear IM model with two state variables: torque and stator flux linkage magnitude. The axiomatically linear model is used to implement a DTC-type controller that maintained all DTC merits and eliminates the flux linkage and torque ripples effect. However, feedback linearization approaches involve complex implementations which overshadow the simple structure of DTC.

In this paper, a compromise is made between complexity and cost on one side and performance quality on the other side. Therefore, the selection of flux estimation model is made to minimize the drive cost by utilizing specific available sensors. The speed sensor is needed in elevator applications where smooth low-speed operation should be guaranteed and is not affordable satisfactorily by speed-sensorless schemes. Cost reduction is also realized by avoiding additional hardware that would be needed if specific estimation models are selected. In case of the voltage-based model is used, expensive stator voltage sensors [21], or stator voltage reconstruction hardware [22] or algorithms that require precise inverter parameters would be needed to account for inverter nonlinearity. Therefore, in this paper current-model based flux estimation is used in which two stator currents, DC voltage, and rotor speed are all the required measurements.

Speed profiling for a comfortable ride is presented. Also, the logic of the necessary supervisory control signals based on only two master elevator's control signals (ON/OFF and UP/DOWN) is developed. These supervisory control signals are responsible for accurate timing/sequencing of operational activities such as gradual building the motor flux, releasing the motor brake in tandem with activating the speed controller and producing the traction torque, reactivating the brake, and gradual removal of machine flux upon reaching the standstill.

The drive performance is then presented and investigated using side-by-side comparison of simulation and experimental results. The critical factors affecting performance are also highlighted.

This paper is organized as follows; Section 2 presents the squirrel cage IM model in stator stationary frame which is used to simulate the motor, also it presents the current-model flux estimator. Section 3 explains the implementation of the SVM-DTC. The designs of flux, torque, and speed controllers are explained in section 4. In section 5, some aspects of particular importance to elevator traction are highlighted. The drive performance is examined through the experimental results in section 6 and section 7 has the conclusion.

2. Induction Motor Model and Current-Based Flux Estimator

The squirrel cage induction motor model in the stator stationary frame ($\alpha\beta$-frame) is given as follows [23]:

The motor voltage equations are in (1)-(4):

$$V_{s\alpha} = R_s I_{s\alpha} + \frac{d\psi_{s\alpha}}{dt} \tag{1}$$

$$V_{s\beta} = R_s I_{s\beta} + \frac{d\psi_{s\beta}}{dt} \tag{2}$$

$$0 = R_r I_{r\alpha} + \frac{d\psi_{r\alpha}}{dt} + p\Omega_m \psi_{r\beta} \tag{3}$$

$$0 = R_r I_{r\beta} + \frac{d\psi_{r\beta}}{dt} - p\Omega_m \psi_{r\alpha} \tag{4}$$

The flux linkage equations are as follows:

$$\psi_{s\alpha} = L_s I_{s\alpha} + L_m I_{r\alpha} \quad (5)$$

$$\psi_{s\beta} = L_s I_{s\beta} + L_m I_{r\beta} \quad (6)$$

$$|\psi_s| = \sqrt{\psi_{s\alpha}^2 + \psi_{s\beta}^2} \quad (7)$$

$$\theta_{\psi s} = atan2\left(\psi_{s\beta}, \psi_{s\alpha}\right) \quad (8)$$

$$\psi_{r\alpha} = L_r I_{r\alpha} + L_m I_{s\alpha} \quad (9)$$

$$\psi_{r\beta} = L_r I_{r\beta} + L_m I_{s\beta} \quad (10)$$

$$|\psi_r| = \sqrt{\psi_{r\alpha}^2 + \psi_{r\beta}^2} \quad (11)$$

The electromagnetic torque T_{em} can be expressed as:

$$T_{em} = \frac{3p}{2}\left(\psi_{s\alpha} I_{s\beta} - \psi_{s\beta} I_{s\alpha}\right) \quad (12)$$

The motion equation is:

$$\frac{d\Omega_m}{dt} = \frac{1}{J}\left[T_{em} - T_L - B\Omega_m\right] \quad (13)$$

The previous set of equations involving flux and currents can be rearranged to use the stator currents and the speed ($I_{s\alpha}$,$I_{s\beta}$,Ω_m) as known inputs and the fluxes ($\psi_{s\alpha}$, $\psi_{s\beta}$, $\psi_{r\alpha}$, $\psi_{r\beta}$) as outputs as follows:

$$\psi_{s\alpha} = \sigma L_s \left[I_{s\alpha} + \frac{L_m}{\sigma L_s L_r} \psi_{r\alpha} \right] \quad (14)$$

$$\psi_{s\beta} = \sigma L_r \left[I_{s\beta} + \frac{L_m}{\sigma L_s L_r} \psi_{r\beta} \right] \quad (15)$$

$$\frac{d\psi_{r\alpha}}{dt} = -R_r I_{r\alpha} - p\Omega_m \psi_{r\beta} \quad (16)$$

$$\frac{d\psi_{r\beta}}{dt} = -R_r I_{r\beta} + p\Omega_m \psi_{r\alpha} \quad (17)$$

$$I_{r\alpha} = \frac{1}{\sigma L_r}\psi_{r\alpha} - \frac{L_m}{\sigma L_s L_r}\psi_{s\alpha} \quad (18)$$

$$I_{r\beta} = \frac{1}{\sigma L_r}\psi_{r\beta} - \frac{L_m}{\sigma L_s L_r}\psi_{s\beta} \quad (19)$$

Eqs. (14) to (19) constitute the mathematical basis of the flux estimator shown in Fig. 1, these equations in its presented form involve algebraic loops. Therefore, it is necessary to adopt a recursive solution by inserting one sample time lag after the integrators which provide the values of $\psi_{r\alpha}$ and $\psi_{r\beta}$. This is quite natural since the motor starts with zero rotor flux, but the stator flux is established first by stator currents circulation as indicated in (14) and (15) due to the applied stator voltages. This gives the accuracy of the stator current measurement controlling role in deciding the estimator accuracy. The stator flux induces rotor voltages and hence circulates rotor

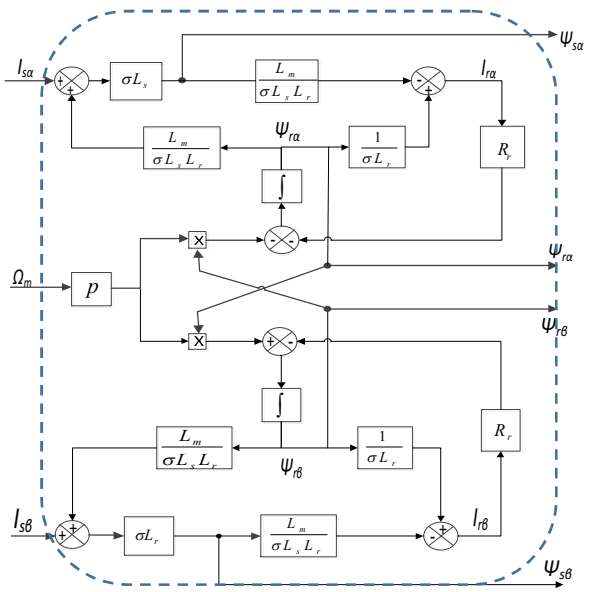

Fig. 1 Current model based flux estimator

currents as indicated in (18) and (19). Once currents start to circulate in rotor circuit, the rotor flux is established as indicated in (16) and (17). Due to the existence of stator and rotor fluxes, the motor torque starts to develop and the rotor starts to rotate, the rotational speed Ω_m affects the rotor flux and consequently the stator flux, and so on. The point here is the accuracy of the instantaneous rotational speed measurement is very decisive in the overall estimator performance. Another issue to be mentioned is that the accuracy of motor parameters also decides the estimator accuracy, however, the estimator sensitivity to current and speed measurement errors is higher compared to its sensitivity to motor parameters error as tested in simulation.

3. SVM-DTC Implementation

The key idea of DTC is that the stator flux response is too fast compared to the rotor flux response. At any rotational speed both stator flux magnitude and angle with respect to rotor flux can be controlled. In other words, the rotor flux can be considered as entirely existing in the *d*-axis of the stator flux synchronously rotating frame and the stator flux component which is responsible for torque production can be controlled instantaneously to control the developed electromagnetic torque by maintaining fixed rotor flux magnitude. In fact the *q*-axis stator flux (orthogonal to rotor flux) controls the torque producing angle and hence the torque can be independently controlled while keeping the *d*-axis flux constant. Therefore, controlling the *q*-axis voltage will control the torque, and controlling the *d*-axis voltage will control the flux magnitude.

Consequently, control will take place in the stator synchronously rotating frame and hence the traditional PI

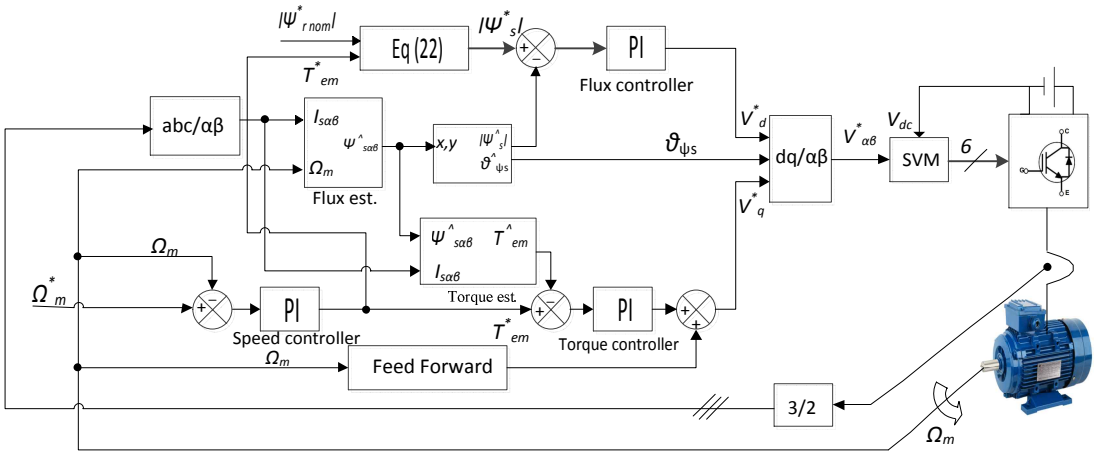

Fig. 2 SVM-DTC control scheme of SCIM

controllers can be used. The angle $\theta_{\psi s}$ is the angle used for transforming the *dq* voltages commands into *αβ* voltages using inverse Park transform.

Fig. 2 depicts the whole control scheme, flux and torque are estimated using the estimator shown in Fig. 1 by receiving the stator current and rotational speed measurements. The speed control loop compares the actual speed to the reference speed and issues the torque command. A PI torque controller compares the estimated torque with the commanded torque and issues a reference *q*-axis voltage. The *q*-component of the electromotive force resulting from the stator flux that is given by $|\psi_s|\omega_{\psi_s}$ and is added to the torque PI output (feed forward) compensation to improve the dynamic response of the torque controller. Since the slip in DTC control is always small, i.e. $p\Omega_m \cong \omega_{\psi_s}$, the measured speed can be used in feed forward instead of differentiating the stator flux angle $\theta_{\psi s}$.

A PI flux controller compares the estimated flux magnitude with the commanded flux magnitude and issues a reference *d*-axis voltage.

To improve the dynamic response of the drive, and to support decoupled control of torque and flux, the rotor flux should be kept constant in magnitude no matter how much torque is developed by the machine. From the *dq*-model of the SCIM when $\psi_{rq} = 0$, the stator flux linkages in *dq*-frame ψ_{sd}, ψ_{sq} can be obtained as in (20) and (21) [23]:

$$\psi_{sd} = \frac{L_s}{L_m}\left(\psi_r + \frac{L_r}{R_r}\sigma\frac{d\psi_r}{dt}\right) \tag{20}$$

$$\psi_{sq} = \frac{2}{3p}\frac{L_r}{L_m}\sigma L_s\frac{T_{em}}{\psi_r} \tag{21}$$

To maintain $\frac{d\psi_r}{dt}$ =0(i.e. maintaining constant rotor flux), it is therefore required to set the reference of stator flux magnitude according to (20) and (21) as in (22):

$$|\psi_s|^* = \sqrt{\psi_{sd}^{*2} + \psi_{sq}^{*2}} = \sqrt{\left(\frac{L_s}{L_m}\psi_r^*\right)^2 + \left(\frac{2}{3p}\frac{L_r}{L_m}\sigma L_s\frac{T_{em}^*}{\psi_r^*}\right)^2} \tag{22}$$

The *d* and *q*-axis reference voltages are converted back to *αβ*-frame using $\theta_{\psi s}$ and the inverse Park transform.

The resulting *αβ*-voltages are used to drive an SVM algorithm in which the switching frequency is predefined, the DC voltage is acquired through measurement. The output of the SVM module is the three duty ratios sent to the PWM module of the H/W in real time setup or to its counterpart in the simulation.

4. Controllers Design

The flux and torque controllers design are based on the assumption that the used scheme sufficiently decouple the torque and flux loops due to fixing the rotor flux.

4.1 Stator flux controller

If the resistive voltage drop is neglected, the transfer function between the *d*-axis voltage and the flux magnitude is simply an integrator as illustrated in (23). The inverter transfer function can be approximated as in (24):

$$\frac{\psi_s}{V_d} = \frac{1}{S} \tag{23}$$

$$\frac{V_d}{V_d^*} = \frac{e^{-ST_d}}{(1+ST_s)} \tag{24}$$

where T_d is the time delay used to avoid shoot through in inverter legs and T_s is the sampling period for the discrete controller. The flux control loop is shown in Fig. 3.

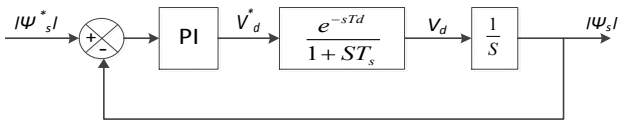

Fig. 3 Flux control loop

According to the symmetry criterion for controller design [23], and provided that T_d is too small compared to T_s (in this paper: 2 and 50, μs respectively), the PI used for flux control might have the following proportional and integral gains in (25) and (26):

$$K_{p\psi} = \frac{1}{2T_s} \tag{25}$$

$$K_{i\psi} = 4T_s \tag{26}$$

It should be mentioned that the smaller T_s, the closer the system to quasi-continuous assumption and hence, the better controller performance.

4.2 Torque controller

A second order open loop transfer function between the torque and the *q*-axis voltage can be expressed as follows [23]:

$$G_T(s) = \frac{T_{em}}{V_q} = \frac{A_T S}{S^2 + B_T S + C_T} \tag{27}$$

where: $A_T = \frac{3p\psi_s}{2\sigma L_s}$, $B_T = \frac{R_s L_r + R_r L_s}{\sigma L_s L_r}$, $C_T = \frac{3p^2 {\psi_s}^2}{2\sigma L_s J}$

The torque control loop is depicted in Fig. 4. The root locus method can be used to design the controller parameters. The single input single output (SISO) control design tool in MATLAB has been used to design the torque PI parameters used in the simulation, however, finer tuning is made by trial and error to reach the best system performance for the experimental setup ($K_{pT} = 40$, $K_{iT} = 140$).

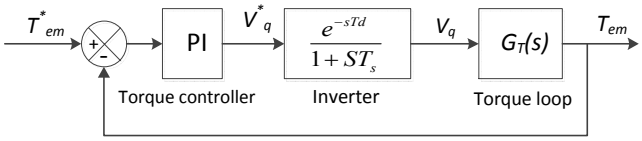

Fig. 4 Torque control loop

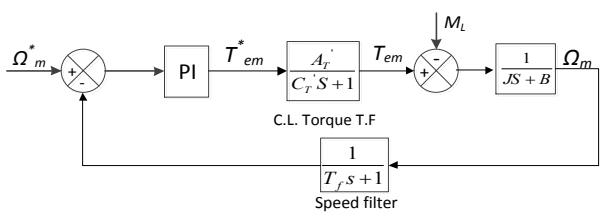

Fig. 5 Speed control loop

4.3 Speed controller

The speed control loop is depicted in Fig. 5, The closed loop transfer function of the torque control loop is approximated to a first order system as in (28) [23].

$$G_T'(s) = \frac{A_T'}{C_T' S + 1} \tag{28}$$

where: $A_T' = \frac{A_T K_{pT}}{C_T K_{iT} + A_T K_{pT}}$, $C_T' = \frac{A_T B_T K_{pT} K_{iT}}{C_T K_{iT} + A_T K_{pT}}$

A low pass filter (LPF) whose transfer function is shown in Fig. 5 is normally inserted in the speed feedback path. The whole plant transfer function can be approximated to:

$$G(s) = \frac{A_T' e^{-ST_d}}{JS(T_a S + 1)} \tag{29}$$

where T_a is the sum of all time constants including the speed low-pass filter T_f. The symmetry criterion can be used for the design of the speed controller parameter and the controller parameters are given in (30) and (31):

$$K_{ps} = \frac{J}{2T_a} \tag{30}$$

$$K_{is} = 4T_a \tag{31}$$

Since *J* is variable in elevators, a fine tuning procedure should be allowed to obtain the best operation for the whole range of *J*.

5. Issues Specific to Elevator Application

5.1 Speed profiling

For a comfortable elevator ride, speed should track a predefined profile starts from zero to the rated speed. To mitigate the impact of the inertial and jerk forces on the passengers, acceleration ramps from zero to the maximum allowable acceleration in a preset interval such that jerk force does not exceed a given limit. Acceleration is then maintained constant for a given interval by the end of which acceleration is ramped down to zero. To plan the speed profile, it is required to set the allowed period (profile period) to accelerate from standstill to the rated speed taken into account the maximum torque capability of the drive. A symmetrical *S*-curve acceleration is illustrated in Appendix 2.

5.2 B. Supervisory controls

A number of issues need to be considered for the safe

and smooth operation of the drive. Since DTC does not involve current control loops, protection based on current measurement should be there to protect the motor and the inverter against any unforeseen control failure. Also, sufficient lag should be allowed between receiving the master traction-ON signal and the inverter activation as to let the slow electromagnetic contactor complete closure on zero current. Then the motor flux should be built according to preset ramp-up rate before enabling the speed acceleration profile or releasing the elevator's brake. Once the torque starts developing, the brake can be released. When the master traction-OFF signal is received, the speed deceleration profile should be enabled, and a speed monitoring should ensure that the minimum speed to brake is reached before activating the brake. Once the brake is activated, the motor flux is allowed to ramp down to zero. Estimated motor flux should be monitored to make sure that the minimum threshold value before disabling the inverter is reached. Then the inverter is disabled and the stator contactor can be de-energized. Breaking the contactor on zero current extends its service lifetime.

All of these considerations can be taken care by some supervisory digital control signals that coordinate the timing of these different activities.

6. Performance Investigation

The drive performance is simulated using MATLAB/ SIMULINK to fine tune the controller parameters. The experimental setup shown in Fig. 6 is used to validate the designed controls and to verify the system overall performance.

A traction type load could not be provided in the laboratory, and hence to load the system, a permanent magnet synchronous generator (PMSG) feeding a resistive load is coupled to the SCIM shaft.

To simulate the load, the PMSG absorbed power is calculated and divided by the rotational speed experimentally. The obtained torque is found to be nonlinear due to the demagnetizing effect of uncontrolled *d*-axis current of the PMSG. A polynomial is found to best fit the relationship between the rotational speed and the torque exerted by the PMSG. This polynomial is used in simulation to reproduce the PMSG torque.

An incremental encoder with 6000 pulses per turn built in the PMSG is used to measure the speed. A two-level three-phase IGBT inverter running at 20 KHz with 2 μs dead time is used to control the SCIM voltages. The control program cycle time is 50 μs. The control task is carried out using dSPACE Microlabox which is a flexible prototyping platform encompassing digital encoder interface and fast A/D converters. The same estimation, coordinate transformation, and control blocks used in the offline simulation are compiled using the real time interface of the dSPACE DSP. The dSPACE control desk is used for on-line visualization of the different system variables. Captures taken from dSPACE control desk are exported to MAT files format and MATLAB plotting functions to reproduce them for comparison with the simulation results.

Speed feedback to the flux estimator should not be filtered otherwise; the accuracy of flux and torque estimation and the whole drive performance in terms of torque ripple is greatly degraded. However, speed feedback to the speed controller should undergo LPF to ensure smooth speed control.

Many simulations have been conducted to test the

(a) The SCIM oupled to PMSG (b) DSP controller

(c) The IGBT inverter

Fig. 6 Experimental Setup

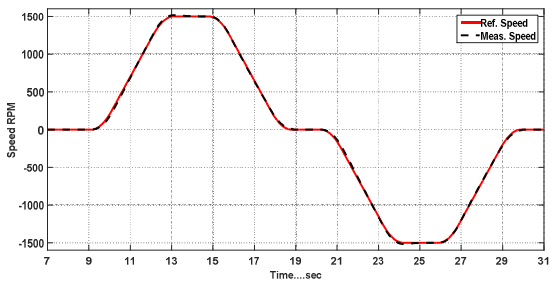

(a) Simulation

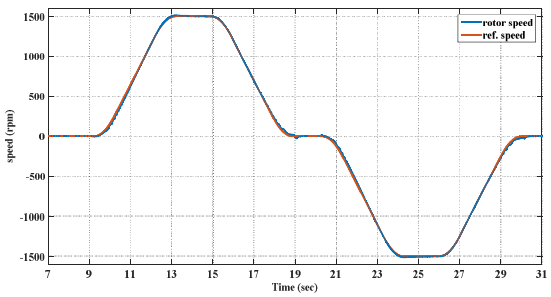

(b) Experimental

Fig. 7 UP/DOWN complete traction cycle speed tracking

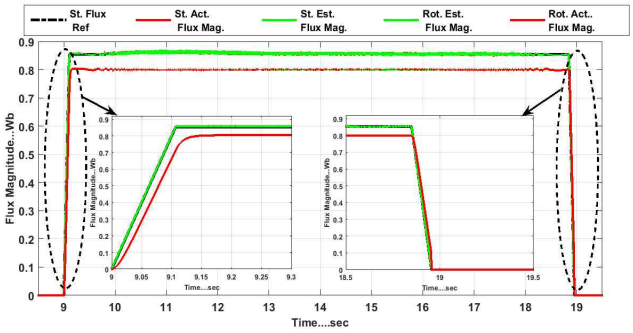

(a) Simulation

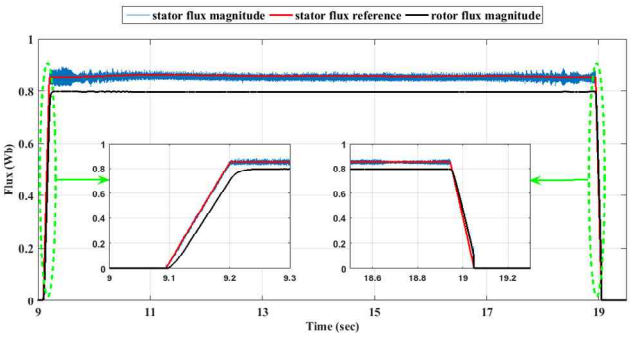

(b) Experimental

Fig. 8 Stator flux controller performance

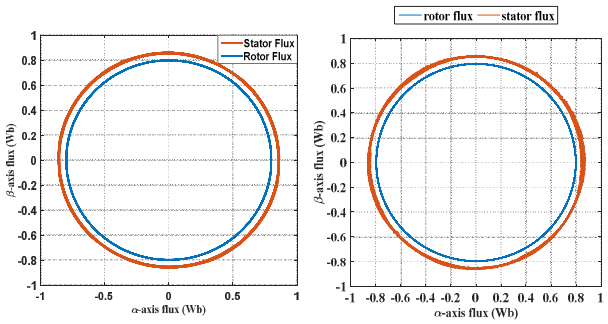

(a) Simulation (b) Experimental

Fig. 9 Stator and rotor flux in $\alpha\beta$-frame

system sensitivity to motor parameter error and to measurement error. It has been found that measurement errors severely degrade the drive performance. The system is relatively tolerable with small motor parameter errors. Fig. 7 shows the speed tracking of the drive. Two traction cycles-up and down-are shown in the case of simulation in subplot (a) and in the case of the experimental setup in subplot (b). The motor speed accurately follows the reference profile in both cases.

Fig. 8 depicts the tracking performance of the stator flux magnitude to its reference value during the ramp-up interval, the constant flux interval and the ramp-down interval. The estimated stator flux satisfactorily tracks the reference value. As explained earlier in (22), the stator flux reference is set such that the rotor flux is maintained

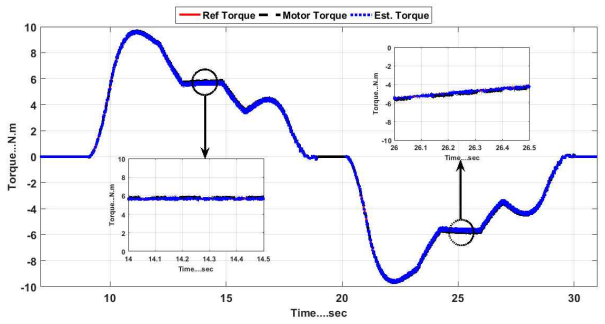

(a) Simulation

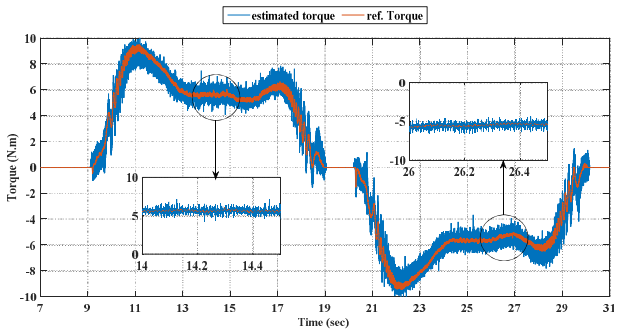

(b) Experimental

Fig. 10 Torque controller performance

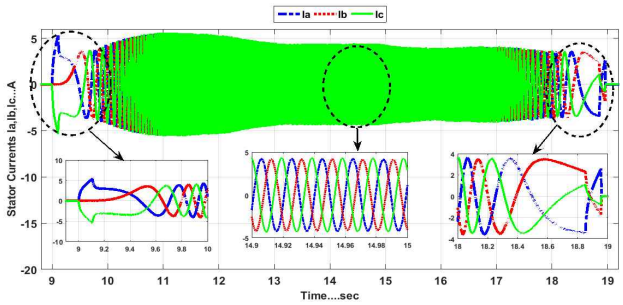

(a) Simulation

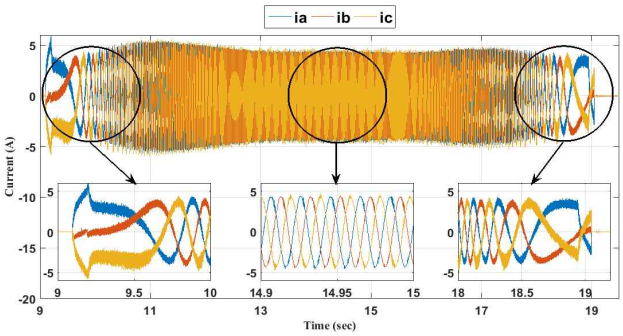

(b) Experimental

Fig. 11 Stator currents

constant at the nominal value (0.8 Wb) which is evident during the constant flux interval. The slower response of the rotor flux which is the enabling feature of the DTC is

evident in the flux ramp-up and ramp-down intervals. Fig. 9 depicts the perfect circular path of both stator and rotor fluxes. Rotor flux has fewer ripples (thin circle) as compared to stator flux (thick circle) due to the filtering effect of the rotor circuit.

Fig. 10 depicts the tracking performance of the torque controller. It is evident that despite the high frequency ripples in the estimated torque, it satisfactorily tracks the reference torque issued by the speed controller. The noisy reference torque assumes that the torque response is too fast as expected from a DTC drive.

Fig. 11 depicts the stator currents during a single traction cycle. Although DTC does not involve direct current control loops, the motor currents are perfect sinusoids. The flux ramping up prior to enabling motion for ensuring that the motor current smoothly grows and is kept within current rating all the time. Also, the gradual collapse of the motor field ensures that the motor contactor is switched off at zero current.

7. Conclusion

DTC is of particular importance for elevator applications. Elevators are distinguished with a need to develop torque at zero speed when the brake is released and with a need to operate at very low speed during acceleration and deceleration intervals of the traction cycle. These requirements cannot be compromised. Therefore, applying sensorless techniques in elevator applications are quite challenging as most of these techniques exhibit low performance at zero and low speeds. Consequently, the majority of high-performance elevator drives are still equipped with speed sensors to maintain high performance under these conditions. DTC equipped with speed sensor has a quite simple structure and it can offer high dynamic performance in terms of torque response time and speed tracking accuracy.

A detailed realization of SVM-DTC controlled IM for elevator applications has been presented. Based on the availability of speed sensor in the elevator motor, flux estimation is carried out using a current model where two stator currents and accurate instantaneous rotor speed is used to overcome the additional cost and complexity usually involved in stator voltage acquisition.

Thanks to the recent achievements of embedded controls and power electronics, nowadays, the high speed and accuracy of the sensors, the high speed of the switching devices, and the high processing speed of the controller required to carry out DTC are no longer regarded as obstacles as compared to the first time DTC was proposed. The high performance of the DTC-scheme presented in this paper is validated through simulation and experimental testing and it confirms the compatibility of the proposed scheme with elevator traction requirements.

Acknowledgements

This work was supported by the Electronics Research Institute – Egypt.

Appendix 1

SCIM Parameters

Parameter	Value	Parameter	Value
Rated power	1500 W	Stator leakage inductance	0.016 H/phase
Rated frequency	50 Hz	Rotor leakage inductance	0.0155 H/phase
No of pair poles	2	Mutual inductance	0.23 H
Rotor phase resistance	2.553 Ω	Full load input current	4.145 A
Friction coeff.	0.008 N.m.s^2	Moment of inertia	0.15 N.m.s

Appendix 2

If the complete period of the *S*-curve profile is T, the ramp up period is T_{up}, the ramp down period is T_{dn}, the constant acceleration period is T_{fx}, the maximum permissible acceleration γ_{max}, the desired maximum speed is Ω_{max} the speed at the end of acceleration ramp up period is Ω_1 and the speed at the end of acceleration ramp up period is Ω_2 following equations describe a symmetrical *S*-curve acceleration profile.

$$T = 4\Omega_{max}/3\gamma_{max} \quad \text{or} \quad \gamma_{max} = 4\Omega_{max}/3T \tag{1}$$

$$T_{up} = T_{dn} = T/4 \tag{2}$$

$$T_{fx} = T/2 \tag{3}$$

$$\Omega_1 = \frac{T.\gamma_{max}}{8} \tag{4}$$

$$\Omega_2 = \frac{5T.\gamma_{max}}{8} \tag{5}$$

In Fig. 2.1, T is selected to be 4 sec. Since the motor rated speed (1500 RPM) is selected to be Ω_{max}, the maximum acceleration γ_{max} is 500 RPM/s, the corner

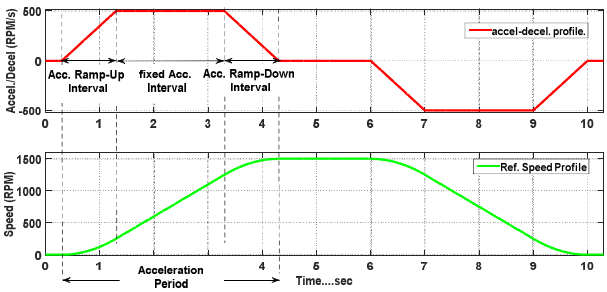

Fig. 2.1 Speed profile for a comfortable ride

speeds Ω_1 and Ω_2 are 250 RPM and 1250 RPM, respectively. Between these two corner speeds, the speed change is linear due to fixed acceleration. By the end of the 4 seconds, the reference speed is 1500 RPM or Ω_{max}. The second subplot is a time integration of the first subplot. The acceleration profile in the first subplot is given to the DSP as a lookup table indexed by time, the timer is activated by the ON/OFF signal to the drive. The positive profile starts upon activating ON signal and the negative profile starts upon activating the OFF signal. The direction signal is used to affect the speed profile signal.

Nomenclature

$V_{s\alpha}$, $V_{s\beta}$	Stator voltages in $\alpha\beta$-frame
$I_{s\alpha}$, $I_{s\beta}$	Stator voltages in $\alpha\beta$-frame
$I_{r\alpha}$, $I_{r\beta}$	The rotor currents in $\alpha\beta$-frame
$\Psi_{s\alpha}$, $\Psi_{s\beta}$	The stator flux linkages in $\alpha\beta$-frame
$\Psi_{r\alpha}$, $\Psi_{r\beta}$	The rotor flux linkages in $\alpha\beta$-frame
Ψ_s, Ψ_r	The stator and rotor flux linkages
$\Psi^*_{r\,nom}$	The nominal flux linkage of the rotor
R_s, L_s	The stator resistance and self-inductance
R_r, L_r	The rotor resistance and self-inductance
σ	The leakage coefficient
L_m	The magnetizing inductance
P	Number of pair poles
J	Inertia of the rotor and connected load
B	Friction coefficient
T_L	Load torque
V_{dc}	The DC-link voltage
Ω_m	The rotor angular speed
Ω^*_m	The reference rotor angular speed

References

[1] C. Lascu, I. Boldea and F. Blaabjerg, "Variable-structure DTC-a class of fast and robust controllers for IM drives," in *IEEE Trans. Ind. Electron*, vol. 51, no. 4, pp. 785-792, Aug. 2004.

[2] G. Wang, and D. Xu, "Robust Low-Cost Control Scheme of Direct-Drive Gearless Traction Machine for Elevators Without a Weight Transducer," in *IEEE Trans. Ind. Appl*., vol. 48, no. 3, pp. 9-16, 2012.

[3] E. Levi, "Multiphase Machines for Variable-Speed Applications," in *IEEE Trans. Ind. Electron*, vol. 55, no. 5, pp. 10-17, 2008.

[4] G. S. Buja and M. P. Kazmierkowski, "Direct torque control of PWM inverter-fed AC motors-a survey," *IEEE Trans. Ind. Electron*., vol. 51, no. 4, pp. 744-757, 2004.

[5] L. Bin, W. Jianru, L. Mingshui and G. Ang, "Research on elevator drive device with super capacitor for energy storage," 2011 *4th International Conference on Power Electronics Systems and Applications*, Hong Kong, 2011, pp. 1-5.

[6] Kuo-Kai Shyu, Ming-Ji Yang and Te Wei Wang "Global Minimum Torque Ripple Design for DTC of Induction Motor Drives," *IEEE Trans. Ind. Electron*., vol. 57, no. 9, pp. 3148-3155, 2010.

[7] M. Ping, "Self-Tuned NFC and Adaptive Torque Hysteresis-Based DTC Scheme for IM," in *IEEE Trans. Ind. Appl*., vol. 50, no. 2, pp. 10-20, 2014.

[8] K. B. Lee and F. Blaabjerg, "Sensorless DTC-SVM for IM driven by a matrix converter using a parameter estimation strategy," *IEEE Trans. Ind. Electron,* vol. 55, no. 2, pp. 512-521, Feb. 2008.

[9] B. El Badsi, and A. Masmoudi, "DTC Scheme for a Four-Switch Inverter-Fed IM Emulating the Six-Switch Inverter Operation," in *IEEE Trans. Ind. Electron*., vol. 28, no. 7, pp. 3528-3538, 2013.

[10] A. Berzoy; J. Rengifo; O. Mohammed, "Fuzzy Predictive DTC of IM with Reduced Torque Ripple and High Performance Operation," in *IEEE Trans. on Power Elect.*, vol. PP, no. 99, pp. 1-10, 2017.

[11] S. S. Sebtahmadi, A. Radan and S. Mekhilef, "A 12-Sector Space Vector Switching Scheme for Performance Improvement of Matrix-Converter-Based DTC of IM Drive," in *IEEE Trans. on Power Elect.*, vol. 30, no. 7, pp. 3804-3817, July 2015.

[12] V. N. N, A. Panda and S. P. Singh, "A Three-Level Fuzzy-2 DTC of Induction Motor Drive Using SVPWM," *in IEEE Trans. Ind. Electron*, vol. 63, no. 3, pp. 1467-1479, March 2016.

[13] C. Ashfak and A. Hareesh, "DTC of four switch three-phase inverter fed IM drive using ANN," 2015 *International Conference on Power, Instrumentation, Control and Computing* (PICC), 2015, pp. 1-7.

[14] Y. N. Tatte and M. V. Aware, "Torque Ripple and Harmonic Current Reduction in a Three-Level Inverter-Fed DTC Five-Phase IM," in *IEEE Trans. Ind. Electron*., vol. 64, no. 7, pp. 5265-5275, 2017.

[15] S. Payami, and A. Iqbal, "DTC of Three-Level NPC Inverter fed Five-Phase IM with Novel Neutral Point Voltage Balancing Scheme," in *IEEE Trans. on Power Elect.*, vol. PP, no. 99, pp.1-10, 2017.

[16] K.-B. Lee and F. Blaabjerg, "An improved DTC-SVM method for sensorless matrix converter drives using an over modulation strategy and a simple non-linearity compensation," *IEEE Trans. Ind. Electron*., vol. 54, no. 6, pp. 3155-3166, 2007.

[17] A. Ammar, A. Bourek and A. Benakcha, "Implementation of robust SVM-DTC for induction motor drive using second order sliding mode control," 2016 *8th International Conference on Modeling, Identification and Control* (ICMIC), Algiers, 2016, pp. 338-343.

[18] F. Ben Salem and N. Derbel, "Investigation of SM DTC-SVM performances of IM control considering load disturbances effects," 2016 *13th International Multi-Conference on Systems, Signals & Devices* (SSD), Leipzig, 2016, pp. 59-65.

[19] F. Wang, W. Xie, and R. M. Kennel, "Model-Based Predictive Direct Control Strategies for Electrical Drives: An Experimental Evaluation of PTC and PCC Methods," in *IEEE Transactions on Industrial Informatics*, vol. 11, no. 3, pp. 671-681, 2015.
[20] C. Lascu, S. Jafarzadeh, and F. Blaabjerg, "Direct Torque Control With Feedback Linearization for IM Drives," in *IEEE Transactions on Power Electronics*, vol. 32, no. 3, pp. 2072-2080, March 2017.
[21] "Isolated Current Shunt and Voltage Measurement for Motor Drives Using," TIDU755-February 2015. Downloaded from: www.ti.com
[22] "Phase Voltage Reconstruction Based on the Qorivva Devices," Freescale Semiconductor, Application Note, Document Number: AN4762. Application Note. Rev 0, 10/2013.
[23] M. Żelechowski, "Space Vector Modulated DTC Inverter – Fed IM Drive," Ph.D. Thesis, Warsaw University of Technology, 2005.

Osama M. Arafa was born in Tanta - EGYPT on December 25, 1965. He graduated from the Electrical Power and Machines Department of the Faculty of Engineering – Minofiya University in 1990. He received M.Sc. and Ph.D. from the faculty of Engineering of Cairo University in 1998 and 2004 respectively. From 2004 to 2011 he worked for several automation companies and is currently working as an associate professor researcher at the Electronics Research Institute – Egypt. His research interests include Power Electronics, Energy Conversion, Control of Electrical Drives and Renewable Energy Systems.

Mohamed E. Abdallah was born in Shoubra-EGYPT on January 3, 1989. He graduated from the Electrical Power and Machines Department of the Faculty of Engineering – Benha University on May 2011. Mohamed received M.Sc. from the faculty of Engineering of Cairo University on 2016. His employment experience included the Egyptian Atomic Energy Authority and Electronic Research Institute. His specific fields of interest include Automatic Control, electrical machine drives and Renewable Energy. He is currently working as assistant researcher at Electronic Research institute – Egypt.

Ghada A. Abdel Aziz received the B.Sc and the M.Sc degrees in Electrical Engineering from Minofiya University, Egypt, in 2006, 2009, respectively, and the Ph.D. degree in Electrical Engineering, Cairo University, Egypt, in 2015. From 2006 to 2008, she was Teaching Assistant with several academic institutions in Egypt. Since 2009, she joined the Electronics Research institute (ERI) in Egypt as a research assistant. From 2015 to present she is a researcher at ERI. Her current research interests include control of electrical machines, power electronics in sustainable energy systems, fault tolerant control, and fault tolerant design of electric machine and power electronics system.